






Could the Migration of Jupiter Have Accelerated the Atmospheric Evolution of Venus?

Stephen R. Kane¹ , Pam Vervoort¹, Jonathan Horner² , and Francisco J. Pozuelos^{3,4} ¹ Department of Earth and Planetary Sciences, University of California, Riverside, CA 92521, USA; skane@ucr.edu² Centre for Astrophysics, University of Southern Queensland, Toowoomba, QLD 4350, Australia³ Space Sciences, Technologies and Astrophysics Research (STAR) Institute, Université de Liège, Allée du 6 Août 19C, B-4000 Liège, Belgium⁴ Astrobiology Research Unit, Université de Liège, Allée du 6 Août 19C, B-4000 Liège, Belgium

Received 2020 April 3; revised 2020 August 7; accepted 2020 August 10; published 2020 September 4

Abstract

In the study of planetary habitability and terrestrial atmospheric evolution, the divergence of surface conditions for Venus and Earth remains an area of active research. Among the intrinsic and external influences on the Venusian climate history are orbital changes due to giant planet migration that have both variable incident flux and tidal heating consequences. Here, we present the results of a study that explores the effect of Jupiter's location on the orbital parameters of Venus and subsequent potential water-loss scenarios. Our dynamical simulations show that various scenarios of Jovian migration could have resulted in orbital eccentricities for Venus as high as 0.31. We quantify the implications of the increased eccentricity, including tidal energy, surface energy flux, and the variable insolation flux expected from the faint young Sun. The tidal circularization timescale calculations demonstrate that a relatively high tidal dissipation factor is required to reduce the eccentricity of Venus to the present value, which implies a high initial water inventory. We further estimate the consequences of high orbital eccentricity on water loss, and estimate that the water-loss rate may have increased by at least ~5% compared with the circular orbit case as a result of orbital forcing. We argue that these eccentricity variations for the young Venus may have accelerated the atmospheric evolution of Venus toward the inevitable collapse of the atmosphere into a runaway greenhouse state. The presence of giant planets in exoplanetary systems may likewise increase the expected rate of Venus analogs in those systems.

Unified Astronomy Thesaurus concepts: [Venus \(1763\)](#); [Exoplanet systems \(484\)](#); [Habitable planets \(695\)](#); [Orbital evolution \(1178\)](#)

1. Introduction

The current state of the Venusian atmosphere and the pathway through which it arrived there is an exceptionally complicated topic. Numerous studies have provided insights into the climate evolution of Venus and discussed primary influences on the atmospheric dynamics (Bullock & Grinspoon 1996; Taylor & Grinspoon 2009; Taylor et al. 2018), including obliquity variations (Barnes et al. 2016). The evolutionary history of the atmosphere of Venus, and its potential divergence from a temperate “Earth-like” climate, depends heavily upon assumptions regarding the initial conditions. For example, Hamano et al. (2013) proposed that Venus may have never had surface liquid water oceans due to an extended magma surface phase. Ramirez (2020) suggested that a high nitrogen inventory on a young planet could lead to a delay in runaway greenhouse scenarios, and that such a scenario might have caused Venus to transition directly into a runaway state without the need for a moist greenhouse. Alternatively, some models suggest that Venus may have had temperate surface conditions that allowed the persistence of surface liquid water until as recently as ~0.7 Ga (Way et al. 2016), depending upon assumptions regarding rotation rates and convection schemes (e.g., Leconte et al. 2013; Ramirez 2018). Such potential for past Venusian surface habitability has been the basis for defining the empirically derived inner edge of the “Habitable Zone” (Kasting et al.

1993; Kopparapu et al. 2013, 2014; Kane et al. 2016). The connection to planetary habitability has further fueled the relevance of Venus to refining models of exoplanets (Kane et al. 2019), both in terms of studying atmospheric chemistry (Schaefer & Fegley 2011; Ehrenreich et al. 2012) and detection prospects for potential Venus analogs (Kane et al. 2013, 2014; Ostberg & Kane 2019).

In the consideration of climate evolution, the orbital parameters of a planet can play a key role in the energy budget distribution over the surface of the planet (Kane & Torres 2017). In particular, it has been demonstrated that the orbital eccentricity can have significant consequences for the climate evolution of terrestrial planets (Williams & Pollard 2002; Dressing et al. 2010; Kane & Gelino 2012; Bolmont et al. 2016; Way & Georgakarakos 2017; Palubski et al. 2020). Overall planetary system architectures can also play a role, such as the effect of Jupiter on impact rates (e.g., Horner & Jones 2008, 2009, 2012) and refractory elemental abundance (e.g., Horner et al. 2009; Desch et al. 2018) in the early inner solar system. Correia et al. (2012) showed that the eccentricity of planetary orbits can be increased by the excitation effects of outer planets that exceed the dampening effects of tidal heating. For those planets where the eccentricity contributes to significant tidal heating, the additional surface energy flux can trigger a runaway greenhouse for an otherwise temperate terrestrial planet (Barnes et al. 2013). Furthermore, the current rotation rate of Venus appears to be impacted by eccentricity and resulting solar tidal torques (Ingersoll & Dobrovolskis 1978; Bills 2005; Green et al. 2019), in addition to interactions between the atmosphere and topography (Fukuhara et al. 2017; Navarro et al. 2018).



Original content from this work may be used under the terms of the [Creative Commons Attribution 4.0 licence](#). Any further distribution of this work must maintain attribution to the author(s) and the title of the work, journal citation and DOI.

At the present epoch, Venus has the lowest orbital eccentricity ($e_V = 0.006$) of the solar system planets and is also in a post-runaway greenhouse state. However, both of these aspects of Venus have a time-evolution component. For example, the eccentricity of the Venusian orbit has both increased due to perturbations from the other planets and decreased due to tidal dissipation. In this paper, we explore the effects of possible giant planet migration on the Venusian orbital eccentricity in the early history of the solar system and the possible impacts on the climate evolution of the planet. In Section 2 we provide the details of our dynamical analysis and the range of eccentricities that Venus could have attained, depending on the location of Jupiter. We further calculate tidal dissipation timescales and show that a significant initial volatile inventory can greatly decrease circularization time frames. Section 3 discusses the consequences of a high Venusian eccentricity, including tidal effects, insolation, and water-loss rates. Section 4 describes the relative effect of eccentricity evolution for both Earth and Venus, including water-loss scenarios. In Section 5 we discuss the potential implications of this analysis for terrestrial planets in systems with giant planets, and we provide concluding remarks in Section 6.

2. Evolution of the Venusian Orbit

2.1. Migration and Formation Scenarios

As we have learned more about the solar system, it has become clear that the giant planets must have migrated during their formation and evolution, before settling at their current locations. Evidence for that migration abounds in the system’s various small body populations. These include the sculpting of the asteroid belt and orbital distribution of the Jovian Trojans (e.g., Morbidelli et al. 2005; Minton & Malhotra 2009, and references therein), and the excitation of the Plutinos and distribution of objects beyond Neptune (e.g., Malhotra 1993, 1995; Hahn & Malhotra 2005; Levison et al. 2008; Lykawka et al. 2009, 2010). Although significant giant planet migration is now firmly established, there remains debate over the extent of that migration, its smoothness or chaoticity, and its timing. Migration models have ranged from the late (~ 700 Myr after planet formation) chaotic interactions of the Nice Model (e.g., Gomes et al. 2005; Morbidelli et al. 2005) to the early but dramatic “Grand Tack” migration of Jupiter and Saturn, in which it is suggested that Jupiter might have migrated inward to approach the current orbit of Mars, before tacking outward to reach its current location (e.g., Walsh et al. 2011; Raymond et al. 2014; Nesvorný 2018)—a process that would have had a significant impact on the hydration of the inner solar system (e.g., O’Brien et al. 2014; Raymond & Izidoro 2017). In particular, the predominant version of the Grand Tack model assumes a disk-dominated migration of Jupiter that was completed before the terrestrial planets formed (e.g., Chambers 2014). Alternatively, models of planetesimal-driven migration of the giant planets can occur over much longer timescales, far beyond the dissipation of the disk required by the Grand Tack model (Hahn & Malhotra 1999; Malhotra 2019). Further migration models consider the possibility of non-uniform, stochastic migration (e.g., Morbidelli et al. 2010; Nesvorný et al. 2018), whereas other models consider more sedate, smoother migration (e.g., Lykawka et al. 2009, 2010; Pirani et al. 2019). Additional complications include evidence via isotopic measurements from meteorites

that suggest terrestrial protoplanets completed accretion quickly and while the gas was still present (Schiller et al. 2018), and the prevalence of proto-atmospheres for terrestrial planets while still present in the gas phase (Mai et al. 2020). A summary of migration and formation models is provided by Raymond & Morbidelli (2020).

Regardless of the true nature of the giant planet migration, the past few decades have seen extensive investigation of the dynamical evolution of the solar system (e.g., Laskar 1988; Duncan & Quinn 1993; Levison & Agnor 2003; Batygin & Laughlin 2008; Brasser et al. 2009; Zeebe 2015). In addition to investigations of an early solar system, dynamical simulations by Laskar (1988) considered the current stability of the solar system, finding that the orbital eccentricities of both Venus and Earth remain largely circular over several-million-year timescales, based on their present orbital parameters. As described previously, several theories regarding the formation and migration of the giant planets, Jupiter and Saturn, suggest that there may have been periods during which they were significantly closer to the Sun, including the Nice model (Gomes et al. 2005; Tsiganis et al. 2005) and the complementary Grand Tack model (Walsh et al. 2011, 2012). Given the aforementioned variety in migration theories discussed in the literature, the effects of that migration on the inner solar system are now the subject of investigation. It has been suggested that the dynamical stability of the terrestrial planets may serve as a useful discriminant between the different Jupiter migration models (Nesvorný 2018), with such models considered likely to help explain the relatively high eccentricity of Mercury’s orbit (Roig et al. 2016).

The purpose of this work is not to evaluate the relative merits of these and other similar models, but rather to assess the impact of Jupiter’s location on the orbital dynamics of the inner planets. However, it is worth noting that our model largely depends on Jupiter’s migration occurring after Venus’s formation is complete or a proto-Venus that retains eccentricity from formation processes. Numerous models described herein allow for these possibilities, and so the subsequent discussion describes the results of a detailed dynamical simulation and the implications for the orbital eccentricity of Venus.

2.2. Dynamical Simulation

The dynamical simulations required for this study were conducted as part of a broader investigation of the degree to which Jupiter’s semimajor axis and eccentricity drive the time-variability of dynamical behavior in the solar system. A detailed description of the dynamical simulations can be found in Horner et al. (2020), which concentrated on the effect of Jupiter on the Milankovitch cycles of the Earth. Here we provide a brief description of the simulations and the components of the simulation that are utilized in this study.

The full suite of simulations was constructed using N -body integrations calculated using the Hybrid integrator within the MERCURY N -body dynamics package (Chambers 1999). The simulations included the eight major planets of the solar system and incorporated the current orbital elements extracted from the Horizons DE431 ephemerides (Folkner et al. 2014). The full suite of simulations covered a large grid of Jupiter semimajor axes (3.2–7.2 au) and eccentricities (0.0–0.4), totaling 159,201 simulations. Each simulation was run for 10^7 simulation years, with a time step of 1 day to ensure perturbation accuracy, and first-order post-Newtonian relativistic corrections were

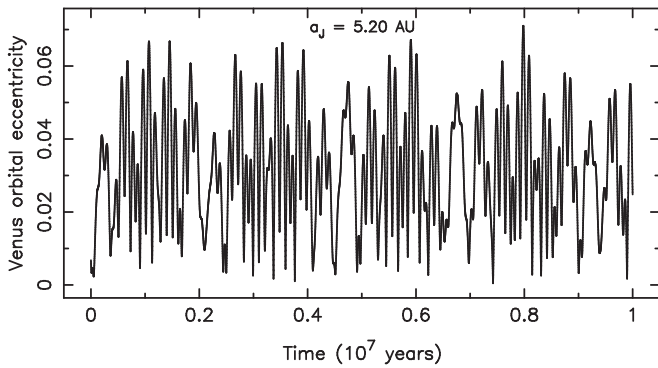


Figure 1. Orbital eccentricity of Venus as a function of time for the present solar system configuration ($a_J = 5.20$ au). Time zero corresponds to the current epoch when the eccentricity resides at a periodic low point. The eccentricity peaks at a value of 0.07 and exhibits high-frequency and low-frequency variations, with periods of 4.1×10^5 yr and 2.2×10^6 yr, respectively.

accounted for (Gilmore & Ross 2008). The output of each simulation was recorded with a time step of 1000 yr. Simulations were halted early if any of the planets became “lost,” including collisions with the Sun or each other, or moving beyond a heliocentric distance of 40 au.

Our study of Venus uses 399 of the total simulation set, and includes starting orbital parameters of Jupiter with zero eccentricity in the semimajor axis range $a_J = 3.2\text{--}7.2$ au. We restricted this study to those simulations for which the initial eccentricity of Jupiter’s orbit was zero, in order to minimize assumptions regarding the potential migration scenarios for Jupiter and to focus our work on the influence of the giant planet’s location alone.

2.3. Eccentricity of the Venusian Orbit

As noted in Section 1, the present orbital eccentricity of Venus is the lowest of all solar system major planets, with a value of 0.006. The results from our simulation for the case of a Jupiter semimajor axis of 5.20 au and eccentricity of 0.048 (present configuration) are shown in Figure 1. These results demonstrate that the present orbital eccentricity of Venus is at a periodic low point, with the maximum value of the periodic eccentricity oscillations of ~ 0.07 in agreement with the results from Laskar (1988) and Bills (2005). A Fourier analysis of the data represented in Figure 1 revealed that the eccentricity variations exhibit high-frequency periodicity of 4.1×10^5 yr and a low-frequency periodicity of 2.2×10^6 yr, primarily a result of perturbations from the Earth and Jupiter. For comparison, the eccentricity of the Earth varies in the range 0.0034–0.058 and is currently 0.0167 (Laskar 1988), the variations of which were also validated by our model (Horner et al. 2020).

The relatively mild variations in the orbital eccentricity of Venus exhibited in Figure 1 are sensitive to the location of Jupiter. Using the results of our extensive suite of dynamical simulations, we extracted the minimum and maximum orbital eccentricities attained by Venus for the full range of Jupiter semimajor axis values. These results are shown in Figure 2, where the dotted (blue) and solid (red) lines indicate the minimum and maximum eccentricity, respectively, for the given Jupiter semimajor axis. The present location of Jupiter is shown as a vertical dashed line. The top axis provides the equivalent period ratio between Jupiter (P_J) and Venus (P_V) as a guide for possible resonance sources of instability.

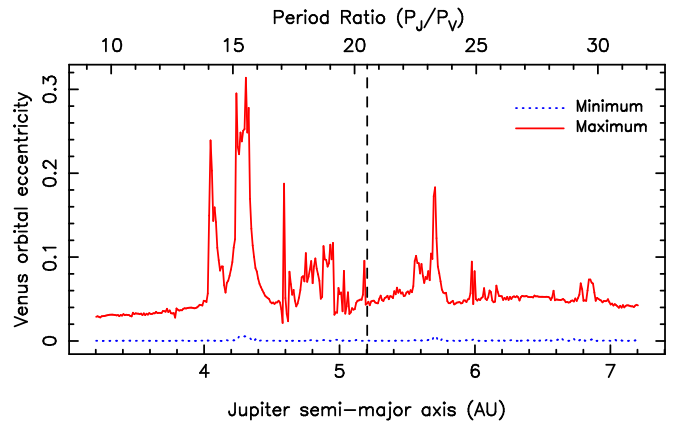


Figure 2. Orbital eccentricity of Venus as a function of the semimajor axis of Jupiter. The dotted (blue) and solid (red) lines indicate the minimum and maximum eccentricities, respectively, that occur during the simulation for the shown Jupiter semimajor axis. The vertical dashed line indicates the present location of Jupiter. The top axis shows the corresponding period ratio between Jupiter (P_J) and Venus (P_V).

The eccentricity data shown in Figure 2 demonstrate the non-trivial relationship between the location of Jupiter and the orbital variability of Venus. It also shows that there are numerous locations at which the influence of Jupiter would cause the range of eccentricity values for Venus to be significantly larger than the present range shown in Figure 1. For example, at $a_J = 5.18$ au, only 0.02 au away from its present location, the maximum eccentricity of Venus rises to 0.10. There are also Jupiter locations farther from its present position that result in large increases in the maximum eccentricity, most particularly at $a_J = 5.71$ au, where the maximum Venusian eccentricity rises to 0.18.

However, it is evident from the eccentricity data that the most powerful perturbations to the Venusian orbit occur when Jupiter is located in the vicinity of $a_J \sim 4.3$ au. The maximum Venusian eccentricity of 0.31 occurs at a Jupiter semimajor axis of $a_J = 4.31$ au. It should be noted that not all of the simulations represented in Figure 2 are dynamically viable for the full 10^7 yr duration. Moreover, as noted by Horner et al. (2020), placing Jupiter at ~ 4.3 au produced instability within the system at all Jovian eccentricities, even zero. Even so, those models of planetary migration that invoke extreme excursions in Jupiter’s orbital elements (such as the Grand Tack model) require the planet to have moved through this location, albeit probably on timescales that allow unstable regions to be effectively circumnavigated, and so such locations and resulting eccentricities are potentially valid regions of exploration.

The case of $a_J = 4.31$ au is shown in Figure 3, where the simulation halted after 1.6×10^6 yr. Placing Jupiter at this particular location has little effect on the orbits of Mars and Saturn, but Figure 3 shows that angular momentum is transferred from Jupiter to Earth and then subsequently passed to Venus, as the orbital eccentricities oscillations of Venus and Earth are directly out of phase with one another. This further demonstrates that although $a_J = 4.31$ au does not appear to correspond to a significant mean motion resonance location (see Figure 2), the chain of perturbations between Jupiter, Earth, and Venus produces exceptionally nonlinear eccentricity distributions.

As a final example, among those simulations for which the solar system remained stable for the full 10^7 yr duration of our

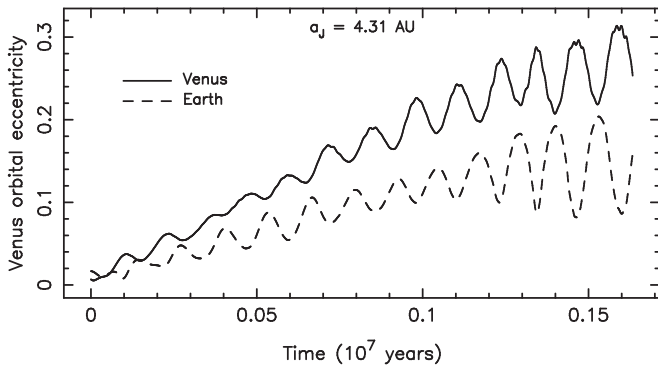


Figure 3. Orbital eccentricity of both Venus (solid line) and Earth (dashed line) as a function of time when Jupiter is located at a semimajor axis of 4.31 au. This particular simulation halted early due to the system instability criteria being met at 1.6×10^6 yr (see Section 2.2).

simulations, the highest values for the Venusian eccentricity occur when Jupiter is located at $a_J = 4.05$ au. The results for the orbital evolution of Venus in this case are shown in Figure 4. The planetary orbit experiences high-frequency oscillations and achieves an eccentricity as high as 0.24, but remains stable nonetheless. Such cases can therefore accommodate a broader range of Jupiter migration models.

2.4. Circularization of the Orbit

If Venus once had an orbital eccentricity as high as 0.31, then the question remains as to how the orbit circularized to its current state. One of the most efficient mechanisms to circularize a planetary orbit is through tidal interactions between the planet and its host star. Using a simple single-planet circularization model based on the methodology described by Goldreich & Soter (1966), the tidal circularization timescale is far older than the age of the solar system. However, numerous other factors, including mutual interactions between planets, contribute to tidal dissipation that reduces the tidal circularization timescale (Laskar et al. 2012). Hence, to include both planet–planet interaction and tides in our study, we made use of the POSIDONIUS N -body code (Bolmont et al. 2015; Blanco-Cuaresma & Bolmont 2017). POSIDONIUS implements the constant time-lag model (CTL) to account for tidal interactions, where a planet is modeled as a weakly viscous fluid that is deformed due to the gradient of the gravitational potential of the central body (i.e., the host star; see, e.g., Mignard 1979; Hut 1981; Eggleton et al. 1998; Leconte et al. 2010). The implementation of this model in POSIDONIUS has been successfully used in a number of recent studies (see, e.g., Bolmont et al. 2020; Nielsen et al. 2020; Pozuelos et al. 2020). It is interesting to note that an alternative tides model exists, namely the constant phase model (CPL), which may yield faster tidal dissipation timescales relative to those found via CTL. We refer the reader to Barnes (2017) and references therein for a detailed review of existing models used to study the evolution of tides in a planetary context.

The main free parameters in the CTL model are the degree-2 potential Love number, k_2 , and the constant time lag, $\Delta\tau$, of each considered planet. While the k_2 parameter accounts for the self-gravity and elastic properties of the planet, which can have values between 0 and 1.5, $\Delta\tau$ represents the lag between the line connecting the two centers of mass (star–planet) and the direction of the tidal bulges, which can span orders of magnitudes (Barnes 2017). In the case of the present-day

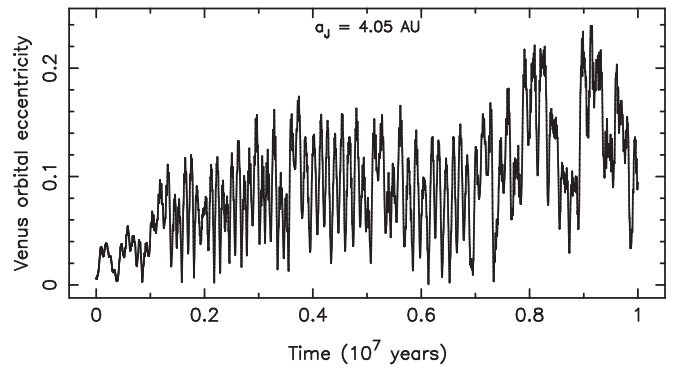


Figure 4. Orbital eccentricity of Venus as a function of time when Jupiter is located at a semimajor axis of 4.05 au.

Earth, the product of these two parameters (i.e., $k_{2,\oplus}\Delta\tau_{\oplus}$) has been estimated to be ~ 213 s (Neron de Surgy & Laskar 1997).

It has been demonstrated that tidal dissipation on present-day Earth is mostly dominated by friction induced by its seafloor topography on tidal gravito-inertial waves that propagate in the oceans (see, e.g., Egbert & Ray 2000, 2003). However, on icy-moons such as Enceladus, tidal dissipation occurs in the sub-surface ocean(s) (e.g., Hay & Matsuyama 2017, and references therein). Thus the tidal braking of an Earth-like planet is mostly dependent on the unknown properties of any putative oceans, whose properties may evolve over time as a consequence of losing/gaining oceanic mass, changes in continental distribution, seafloor topography, and so forth (Neron de Surgy & Laskar 1997; Barnes 2017). Hence, when exploring the tidal evolution of a terrestrial exoplanet, the most commonly used approach is to adopt Earth’s current value as a reference for a planet with surface oceans, where values in the range of $(0.1\text{--}10) \times k_{2,\oplus}\Delta\tau_{\oplus}$ are used to account for different planetary conditions, such as rocky planets without oceans and those that are volatile-rich, respectively. This range allows us to explore a plausible spectrum of values and behaviors (see e.g., Bolmont et al. 2014, 2020).

In the solar system, k_2 has been measured for several objects, while $\Delta\tau$ is, in general, poorly known. In the case of Venus, from the Magellan mission, the value of k_2 was found to be in the range of 0.23–0.36 (Konopliv & Yoder 1996). Moreover, Dumoulin et al. (2017) computed tidal viscoelastic deformation using different models of internal structure, and established k_2 in the range of 0.265–0.270 when a solid pure-iron core was considered and 0.27–0.29 when the core was partially or entirely liquid. These values of k_2 are similar to that found for Earth, which was estimated to be ~ 0.298 (Jagoda et al. 2018). Hence, as a plausible value for present-day Venus (i.e., a rocky terrestrial planet without oceans), we assumed $0.1 \times k_{2,\oplus}\Delta\tau_{\oplus}$.

With all this information, we explored the circularization of the Venus orbit by performing a suite of simulations considering three different scenarios within the solar system: (1) initial Venusian orbital eccentricity excited to 0.31 but with no tidal forces; (2) initial Venusian orbital eccentricity excited to 0.31 and $0.1 \times k_{2,\oplus}\Delta\tau_{\oplus}$ (i.e., the plausible current value representing Venus’s tidal dissipation); and (3) initial Venusian orbital eccentricity excited to 0.31 and $200 \times k_{2,\oplus}\Delta\tau_{\oplus}$. The scenario (3) tidal dissipation of $200 \times k_{2,\oplus}\Delta\tau_{\oplus}$ is unrealistic but accelerates the circularization process and allows us to explore the possible timescale of circularization due to the effects of tides. Indeed, as the timescales of the tidal effects scale linearly with $\Delta\tau$, we are able to estimate the

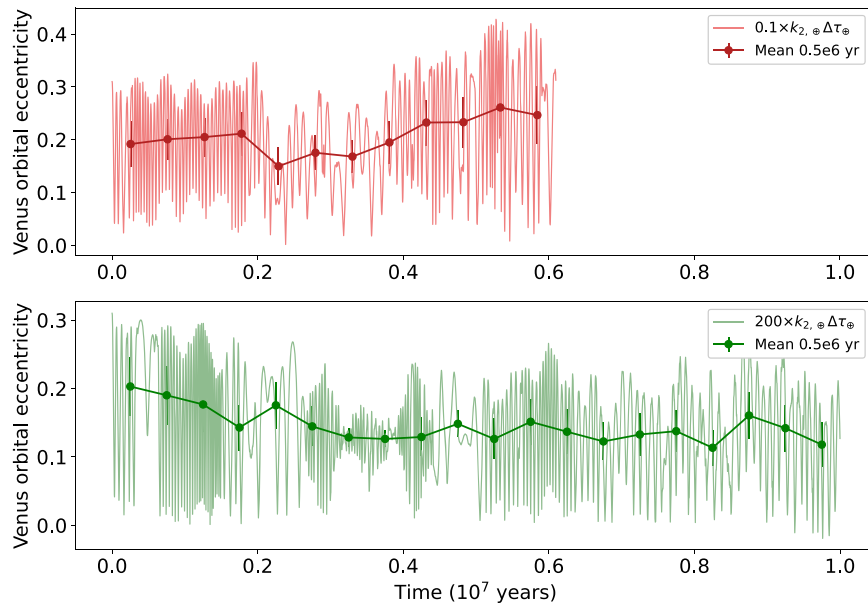


Figure 5. Venus orbit circularization due to the effects of tides for different scenarios: (1) top panel, which considers the current Venus tidal dissipation of $0.1 \times k_{2,\oplus} \Delta\tau_{\oplus}$; and (2) bottom panel, which considers a value of $200 \times k_{2,\oplus} \Delta\tau_{\oplus}$. While the current tidal dissipation of Venus is insufficient to circularize and stabilize the orbit, a large and unrealistic tidal dissipation circularizes its orbit in a timescale of ~ 30 Myr. This latter result allowed us to estimate realistic bounds on Venus’s past tidal dissipation and circularization times of $1.5\text{--}5 \times k_{2,\oplus} \Delta\tau_{\oplus}$, and $4000\text{--}1200$ Myr, respectively.

circularization time for a range of realistic dissipation factors ($1\text{--}10 \times k_{2,\oplus} \Delta\tau_{\oplus}$) in a straightforward manner by using this result (Neron de Surgy & Laskar 1997; Barnes 2017). For self-consistency, we also included the effects of tides for Mercury, which has a k_2 value of 0.45 (Noyelles et al. 2014). However, for simplicity, we did not account for the tidal effects for other planets beyond Venus. This choice was motivated by the very small tidal effects experience by terrestrial planets in the Habitable Zone (and beyond) around solar-like stars (Heller et al. 2011). We integrated the scenarios described above for 10^7 yr with a time step of 1 day, and we accounted for relativistic corrections.

We found that scenario (1) yielded a system which became unstable within a very short timescale of 2 Myr. This hints that if Venus reached an eccentricity of 0.31 during its early history, some mechanism was needed not only to circularize the orbit to reach its current value but also to stabilize it. In scenario (2), we found that the system was more stable with respect to scenario (1); however, it became unstable after 6 Myr. This suggests that the current tidal dissipation of Venus is not enough to stabilize and circularize its orbit. In scenario (3), the system was stable for the full integration time and the orbit started to circularize by decreasing its initial eccentricity by $\sim 35\%$. To estimate the circularization time needed to reach its current value of 0.006, we performed a linear extrapolation of the eccentricity evolution over 10^7 yr, finding a circularization time of ~ 30 Myr to reach the current value. Making use of the aforementioned linear-scale property of tides, we estimated the circularization times for realistic tidal dissipation as 600 Myr for $10 \times k_{2,\oplus} \Delta\tau_{\oplus}$; 1200 Myr for $5 \times k_{2,\oplus} \Delta\tau_{\oplus}$; 3000 Myr for $2 \times k_{2,\oplus} \Delta\tau_{\oplus}$; and 6000 Myr for $1 \times k_{2,\oplus} \Delta\tau_{\oplus}$. These results hint that the current Earth dissipation is not enough to circularize the Venus orbit on a timescale that is less than the age of the solar system. However, these results also clearly show that slightly larger dissipation factors may be valid. The results corresponding to scenarios (2) and (3) are shown in Figure 5.

Taken together, our results suggest that if Venus’s eccentricity was excited up to 0.31 due to Jupiter’s migration in the early solar system, the effects of tides may have played a key role in circularizing and stabilizing Venus’s orbit. We found that the current value of Venus’s tidal dissipation is not enough to achieve this, suggesting that Venus was not as dry in the past as it is today. To circularize its orbit over the timescale of the age of the solar system (~ 4000 Myr, post gas phase and migrations), the dissipation factor needed is $\sim 1.5 \times k_{2,\oplus} \Delta\tau_{\oplus}$. This suggests that Venus might have had a water-rich past, possibly in the form of surface or sub-surface oceans. Due to the similarities between Venus and Earth, it seems more realistic to speak about surface oceans, such as those found on Earth, but we cannot favor any specific location for the water bodies on ancient Venus due to the limitations of the models used in this study. This result agrees with the current formation theories of the solar system, where it has been surmised that Venus and Earth likely received similar water inventories (see, e.g., Raymond et al. 2006). Moreover, it has recently been suggested by Way & Del Genio (2020) that Venus may have possessed early oceans that could have created significant tidal dissipation over ~ 3000 Myr. While it is not currently possible definitive to ascertain the true tidal dissipation scenario experienced by the early Venus, a plausible range of values seems to be $1.5\text{--}5 \times k_{2,\oplus} \Delta\tau_{\oplus}$, which implies circularization times of $4000\text{--}1200$ Myr.

There are numerous other processes that also contribute to the circularization of the Venusian orbit. Tidal dissipation and circularization are tied to the thermal evolution of the planet, decreasing the circularization timescale as the planet’s interior cools (Driscoll & Barnes 2015). Furthermore, the interaction between the atmosphere and surface, strengthened by recent observations of standing gravity waves, is calculated to be a source of tidal dissipation for the Venus system (Dobrovolskis & Ingersoll 1980; Fukuhara et al. 2017). It should additionally be noted that since the orbital eccentricity oscillations of Venus presented here depend on Jupiter’s location, subsequent Jupiter

migration can further impact the Venusian orbital variations. For example, if Jupiter’s migration occurred on a timescale longer than that of the periodic eccentricity oscillations of the Venus orbit, then this would act to dampen the amplitude and frequency of the oscillations. The summation of these sources provides ample opportunity for the orbit of Venus to arrive at its present state from the significantly non-circular cases described previously.

3. Eccentricity Consequences

The energy budget of the Venusian atmosphere has played a critical role in the evolution of both atmosphere and surface (Titov et al. 2007). Here, we quantify the impact of the eccentricity scenarios described in Section 2.3 on the energy budget of Venus.

3.1. Tidal Energy

As described in Section 2.4, tidal dissipation plays a role in circularizing eccentric orbits with time. The internal heat budget of the Earth is well known to be sourced primarily from radiogenic heating and primordial heat. Radiogenic heating of the Earth’s interior, and the resulting heat flux at the surface, can be calculated using the known mass concentrations of potassium, thorium, and uranium and their corresponding half-lives (Turcotte & Schubert 2002). The current total heat flux at the Earth’s surface is ~ 47 TW (Davies & Davies 2010), but at 4 Ga the radiogenic heating alone produced a heat flux of ~ 80 TW (Arevalo et al. 2009).

A third component of internal heat production is gravitational tides. Tidal heating of planetary interiors and tidal dissipation as a result of orbital perturbations can result in planets remaining tidally active for extended periods (Renaud & Henning 2018). Such heat dissipation contributes to the surface heat flow budget and thus the overall energy budget of the atmosphere. Tidal energy potentially extended the duration of the molten surface scenario for a young Venus, increasing the timescale of hydrodynamic escape described by Hamano et al. (2013). It has been further suggested by Barnes et al. (2009) that tidal heating of short-period planets can result in “Super-Io” outcomes with significant resurfacing, as is potentially the case for CoRoT-7b (Barnes et al. 2010). Under extreme circumstances, tidal dissipation can dramatically alter the course of the atmospheric evolution, such as steering that evolution into a runaway greenhouse state (Barnes et al. 2013).

To perform our tidal heating calculations, we adopt the methodology of Jackson et al. (2008a, 2008b). Specifically, we use the equation for the tidal heating rate, H :

$$H = \frac{63}{4} \frac{(GM_\star)^{3/2} M_\star R_p^5}{(3Q_p/2k_2)} a^{-15/2} e^2, \quad (1)$$

where G is the gravitational constant, M_\star is the stellar mass, R_p is the planet radius, Q_p is the tidal dissipation parameter, k_2 is the Love number, a is the semimajor axis, and e is the eccentricity. Note that Equation (1) applies to radial tides, rather than those tides resulting from non-synchronous rotation. Based on the analysis of Magellan and Pioneer Venus data by Konopliv & Yoder (1996) and the reanalysis of those data by Dumoulin et al. (2017), we use values of $Q_p = 12$ and $k_2 = 0.299$. Equation (1) shows the dramatic dependency of the tidal heating on a . Thus the distance of Venus from the Sun

results in a relatively low rate of heating due to radial tides (see Equation (1)). Specifically, for the maximum eccentricity of 0.31 ($a_J = 4.31$ au scenario) described in Section 2.3, we calculate a tidal heating flux at the surface of Venus of ~ 11 GW. The results of the tidal heating calculations were validated using the tide modules of the Virtual Planet Simulator (Barnes et al. 2020). Although the contribution of the tidal heating to the total atmospheric energy budget is low, it occurred at a time when the contribution from the insolation flux was also significantly lower than that at the present epoch.

3.2. Insolation Flux

The incident (insolation) flux for the solar system planets has evolved with time as the Sun evolves on the main sequence. Such evolution can have a profound effect on the time-dependent insolation flux for terrestrial planets (Kulikov et al. 2007), as is seen in calculations of water loss for planets around M dwarfs (Luger & Barnes 2015). In particular, it is known that the Sun was $\sim 30\%$ less luminous in the early era of the solar system (Gough 1981), during which the radiation environment of Venus was substantially different.

To simulate the expected insolation flux of Venus during a possible early era with the high eccentricity described in Section 2.3, we adopt a solar luminosity that is 75% of the current value. At the semimajor axis of Venus, this results in an insolation flux of $S/S_0 = 1.43$, where S_0 is the present-day solar flux received at Earth. One possible scenario is thus the $a_J = 4.31$ au scenario (see Section 2.3), where the evolution of the maximum flux (perihelion) and minimum flux (aphelion) received by Venus is represented in the top panel of Figure 6. As for Figure 3, Venus starts in a circular orbit, then the rise in eccentricity results in a maximum insolation flux that rapidly starts to oscillate high above its present value, indicated by the horizontal dashed line.

To demonstrate the effect of the eccentricity on the flux received at the top of the atmosphere, we simulated the latitudinal flux map of the planet for the case where the eccentricity reaches 0.31 using the methodology of Kane & Torres (2017). The flux map is shown in the bottom panel of Figure 6 as a function of orbital phase, where zero phase corresponds to perihelion passage. We assumed a zero obliquity for the rotational axis and also that the early Venus was a rapid rotator prior to its present near spin-orbit synchronization. The consequence of the assumed rotation means that the incident flux is calculated as an average at each latitude, accounting for the reduced flux as a particular longitude rotates away from maximum solar elevation as well as the zero flux received at the night side of the planet. As such, the average flux values in the contour map are significantly lower than the flux received at the top of the Venusian atmosphere at the sub-solar point. The maximum average flux received (1297 W m^{-2}) therefore occurs at the equator during the perihelion passage. For comparison, the maximum average flux received by the Earth is 563 W m^{-2} . Similarly, the minimum average flux of 360 W m^{-2} occurs at the Venusian equator during aphelion, which is smaller than the minimum average flux received at the equator of the present Earth during its aphelion (386 W m^{-2}).

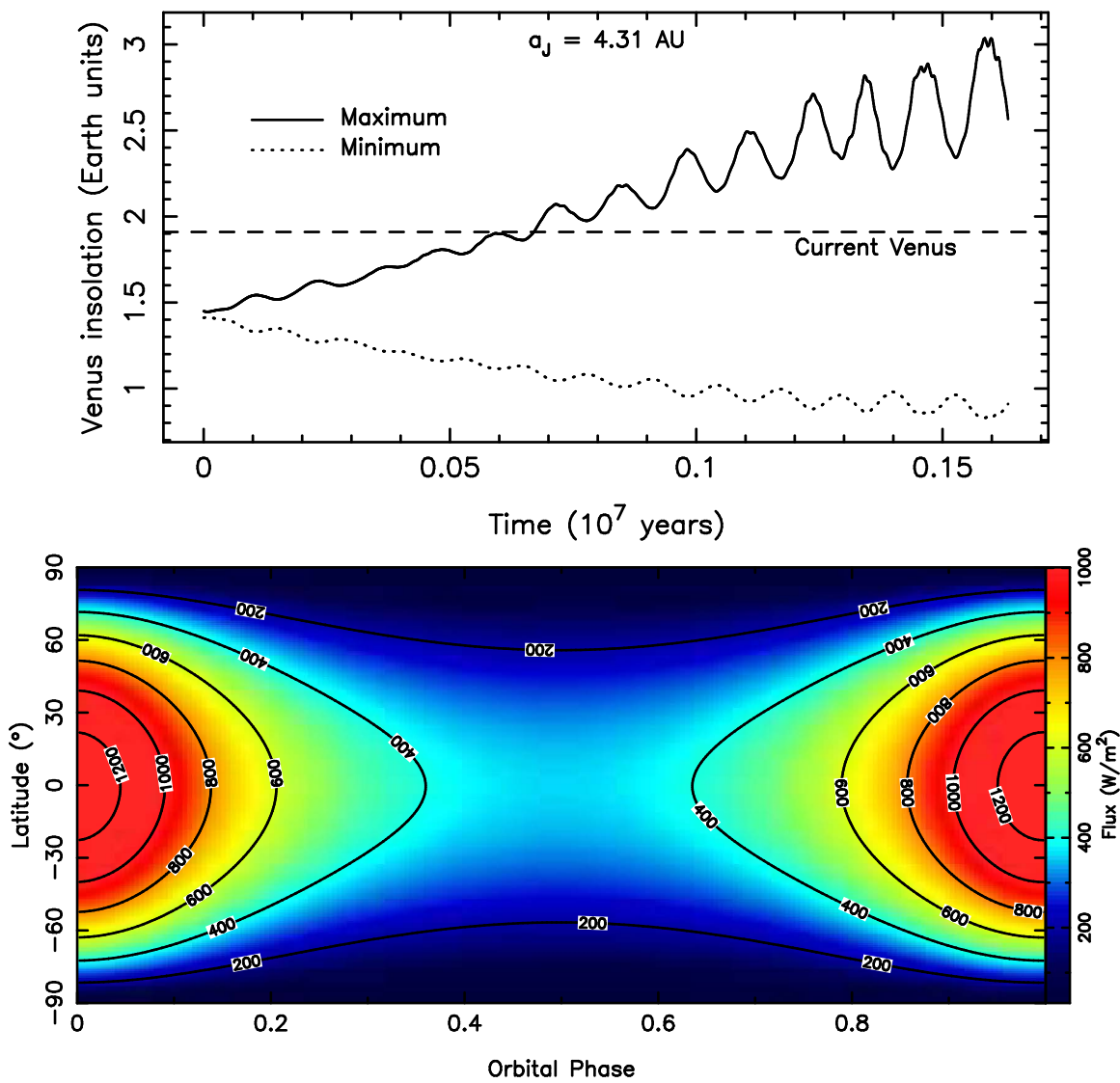


Figure 6. Top panel: maximum insolation (perihelion passage) and minimum insolation (aphelion passage) at Venus as a function of time for the $a_j = 4.31$ au case (see Figure 3). The maximum and minimum fluxes are represented in units of current Earth insolation flux. The horizontal dashed line indicates the insolation flux for current Venus. Bottom panel: diurnal mean incident flux intensity map of Venus for an eccentricity of 0.31 as a function of latitude and orbital phase, where phase zero corresponds to perihelion.

3.3. Water Loss

As described earlier, the loss of water can occur rapidly for planets orbiting M dwarfs (Luger & Barnes 2015), and eccentricity-induced tidal heating can force a runaway greenhouse scenario (Barnes et al. 2013). Significant water loss can also occur during the early period of coronal mass ejection for young solar-type stars (Dong et al. 2017) and the incident XUV flux plays an important role in water loss from CO₂ dominated atmospheres (Wordsworth & Pierrehumbert 2013). Here, we combine several of these aspects to explore the impact of early Venusian eccentricity on the rate at which the planet would have lost its water.

A recent study of the water-loss implications for eccentric orbits conducted by Palubski et al. (2020) used 1D climate models to explore water loss for planets orbiting stars of a range of spectral types. We utilize the data generated for the G2 main-sequence star case, while extending the water-loss calculations to high insolation flux regimes. Shown in Figure 7 are the data for the faint young Sun scenario

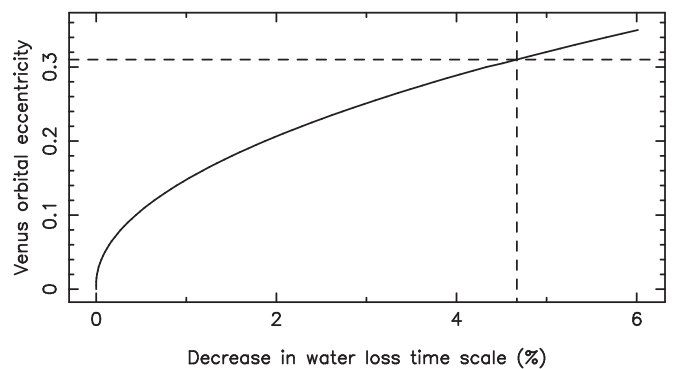


Figure 7. Plot of the decrease in the water-loss timescale for the full range of Venus eccentricities explored in this study. For the maximum eccentricity of 0.31, the timescale to lose one Earth ocean of water decreases by 4.7%, indicated by the dashed lines.

described in Section 3.2, where the insolation flux at the semimajor axis of Venus is $S/S_0 = 1.43$. The horizontal axis is expressed in terms of the percentage effect of eccentricity on the timescale for losing one Earth ocean worth of water (Palubski et al. 2020). For zero eccentricity, this timescale is ~ 3 Gyr. The dashed lines in Figure 7 highlight the water-loss effect for the eccentricity of 0.31 described in Section 2.3. In this case, the time taken to remove all of the water is reduced by 4.7% due to the high eccentricity.

An aspect that is not completely accounted for in the provided water-loss model is the changing luminosity of the Sun. The evolution of the solar luminosity affects the solar wind received by the planets (Pognan et al. 2018), which in turn can have significant effects on atmospheric retention (Ribas et al. 2005; Howe et al. 2020). Furthermore, the pre-main-sequence period of the solar evolution can be characterized by a relatively high XUV flux that also results in substantial atmospheric and water loss (Lammer et al. 2008; Ramirez & Kaltenegger 2014; Gronoff et al. 2020). As a result, the 4.7% reduction in water-loss timescale should be considered a lower limit, and the true water-loss rate would probably be substantially higher as a result of the evolution of the young Sun.

Note that the migration of Jupiter and Saturn likely occurred before 4 Ga, prior to when water would have had an opportunity to be both substantially delivered and condensed on the surface of Venus and Earth. However, the tidal circularization timescale estimated in Section 2.4 demonstrates that the perturbing effect of Jupiter may have had long-lasting consequences. Thus an increased eccentricity for Venus could have been sustained long after Jupiter and Saturn settled to their final (present) locations.

4. Climate Impacts for Earth and Venus

In order to appreciate the possible impacts of eccentricity on Venus, it is worth briefly reviewing the consequences of eccentricity on Earth's climate. Earth's eccentricity oscillates roughly between 0.00 and 0.06, with periodicities of about 100 and 400 kyr resulting from gravitational interactions between Venus (g2), Jupiter (g5), and Mars (g4; Laskar et al. 2004). Both numerical calculations and periodic sedimentary successions found in Earth's geological archive provide evidence that the 405 kyr eccentricity cycle has been stable for at least the past 250 Myr (Laskar et al. 2011; Kent et al. 2018). Despite the small range of variation, some major climatic, environmental, and biological perturbations, driven or paced by these eccentricity variations and the seasonal forcing associated with them, have occurred throughout Earth's history. For instance, during the glacial-interglacial cycles of the past million years, the extent of the North Polar ice cap systematically fluctuated between 80°N and 45°N , with cycles of 100 kyr (Hays et al. 1976; Ehlers & Gibbard 2007). The waxing and waning of ice sheets are related to changes in seasonal insolation at high latitudes. Geological evidence also demonstrates that eccentricity modulation on much longer timescales (~ 2.4 and ~ 9 Myr) has led to the systematic release and sequestration cycles of organic carbon (Boullila et al. 2012; Martinez & Dera 2015; Batenburg et al. 2016; Laurin et al. 2016), which in turn impacted atmospheric greenhouse gas concentrations and, in some cases, possibly led to major perturbation events during which ocean bottom water fell anoxic, leading to the extinction of several marine species (Kuhnt et al. 2005; De Vleeschouwer

et al. 2017). More often than not, astronomically forced perturbations to the Earth's system were related to biological processes impacting the carbon cycle, but the strength of seasonality (i.e., the combined effect of precession and obliquity enforced by eccentricity effects) also plays a crucial role in many other Earth system processes, such as atmospheric heat transport (Donohoe et al. 2013) and ocean dynamics (Lisiecki 2014).

The potential variations of the early Venusian eccentricity may have had severe consequences for climate evolution. Although the tidal energy effects are relatively low (Section 3.1), the insolation flux effects (Section 3.2) and resulting water loss (Section 3.3) may have transferred sufficient water to the atmosphere to accelerate the development of a moist greenhouse (e.g., Kasting et al. 1984; Gómez-Leal et al. 2018). Although CO_2 alone can lead to a non-reversible runaway greenhouse state (Popp et al. 2016), the water distribution between the surface and the atmosphere plays an important role. The insolation flux for the early Venus considered here is 1.43 times the current solar constant, and Kasting (1988) predicted that the insolation flux at which complete water loss occurs is 1.4 times the current solar constant. However, Wolf & Toon (2014), using 3D models rather than the 1D models of Kasting (1988), argued that the onset of a moist greenhouse can occur at significantly higher insolation fluxes. Even so, the water-loss rates presented in Section 3.3 indicate a $\sim 5\%$ reduction in the time to transfer an Earth ocean worth of water to the atmosphere due to enhanced eccentricity, resulting in substantial atmospheric water in the early Venusian atmosphere. For example, $\sim 10^{-3}\%$ of Earth's current surface water inventory resides in the atmosphere. The effect of increasing the atmospheric water content, even by a small amount, can have stochastic climate consequences, depending on the insolation flux and atmospheric composition and structure (Goldblatt 2015). One scenario for a high Venusian atmospheric water content is that it leads to an acceleration of a moist greenhouse, followed by photodissociation (Zahnle & Kasting 1986; Kulikov et al. 2006; Kasting et al. 2015; Lichtenegger et al. 2016). Alternatively, it has been argued that the moist greenhouse phase does not always occur, transitioning directly into a runaway greenhouse (Leconte et al. 2013; Ramirez 2020).

5. Implications for Exoplanets

The architectures of exoplanetary systems is a topic of rapidly advancing research, particularly in light of the expanding inventory and demographics of exoplanet discoveries (Ford 2014; Winn & Fabrycky 2015). Smaller (terrestrial) planets tend to have smaller eccentricities, particularly those in compact systems (Kane et al. 2012). However, the work described here shows that the early stages of architecture evolution may be more turbulent in the presence of a migrating giant planet. Thus giant planets in exoplanetary systems may play a critical role in the development of terrestrial planet climates.

Studies of giant planet occurrence rates at long orbital periods have demonstrated that their frequency is relatively low (Hill et al. 2018; Wittenmyer et al. 2020). Furthermore, observational evidence points toward giant planets being even scarcer around M dwarf stars (Cumming et al. 2008; Johnson et al. 2010). If giant planet migration processes, similar to that undertaken by Jupiter and Saturn, are a common feature of

early planetary system development, then the excitation and subsequent dampening of inner terrestrial planet eccentricities likewise may be common in such systems. The profound implication is that the presence of giant planets in the outer part of planetary systems may increase the likelihood of water loss and runaway greenhouse climate evolution, resulting in a more extensive Venus Zone than previously estimated (Kane et al. 2014). As the sensitivity of exoplanet measurements continue to increase in the long-period regime, and as the atmospheres of Venus analogs are detected, this proposed correlation may be properly evaluated (Lincowski et al. 2019; Lustig-Yaeger et al. 2019).

6. Conclusions

The evolution of the Venusian climate still has many outstanding questions, most particularly as to whether the planet was habitable until relatively recently (Way et al. 2016) or was devoid of surface liquid water from its formation (Hamano et al. 2013). Answering these questions is crucial for understanding not just the comparative evolution of Earth and its sibling planet, but the prevalence and sustainability of planetary habitability in a broad range of exoplanetary systems. There have been many differences between Venus and Earth with regard to their overall planetary evolution, and determining the dominant factors that drove those evolutions remains a topic of active research.




The study presented here specifically investigates the effect of possible orbital dynamical scenarios on the evolution of an early Venus. Our simulations and subsequent analyses demonstrate that (1) the eccentricity of the Venusian orbit is dramatically increased for particular locations of Jupiter and (2) the consequences of the increased eccentricity would have included a significantly increased rate of surface liquid water loss. Clearly there exists a vast parameter space of initial orbital conditions that are possible, of which the study presented here has explored a subset. Furthermore, our simulations do not include the migration effects of Jupiter and Saturn during the course of individual dynamical simulations. The inclusion of specific migration patterns would marginalize the results given the plethora of possible migration scenarios (see Section 2.1). Rather, our methodology considers each simulation as an encapsulated exploration of the perturbative effects of Jupiter as a function of semimajor axis to provide a first-order picture of possible dynamical scenarios during migrational pathways. However, our investigations of tidal dissipation and circularization timescales show that damping the eccentricity perturbations of Venus to their current value requires a larger initial water inventory than that for the current Earth, lending credence to the notion of substantial water delivery to an early Venus.

If Jupiter did indeed accelerate the early climate development of Venus, then similar situations may have occurred elsewhere. The occurrence rate of detectable giant planets near or beyond the snow line is known to be relatively low. However, for those systems with outer giant planets, the early dynamical history of those systems may cause a measurable increase in the occurrence rate of inner terrestrial planets in runaway greenhouse states. Such dynamical impacts on terrestrial climate evolution are thus an important factor in considering planetary evolution and habitability.

The authors would like to thank Sean Raymond for detailed feedback regarding migration and formation models, Cayman Unterborn for discussions regarding planetary interiors, Igor Palubski for communications regarding water-loss models, and Anthony Del Genio for feedback regarding climate evolution. The authors would also like to thank the anonymous referees for their insightful comments on the manuscript. P.V. acknowledges funding support from the Heising-Simons Foundation. The results reported herein benefited from collaborations and/or information exchange within NASA's Nexus for Exoplanet System Science (NExSS) research coordination network, sponsored by NASA's Science Mission Directorate.

Software: Mercury (Chambers 1999), VPlanet (Barnes et al. 2020), Posidonius N-body (Blanco-Cuaresma & Bolmont 2017).

ORCID iDs

Stephen R. Kane  <https://orcid.org/0000-0002-7084-0529>
Jonathan Horner  <https://orcid.org/0000-0002-1160-7970>
Francisco J. Pozuelos  <https://orcid.org/0000-0003-1572-7707>

References

- Arevalo, R., McDonough, W. F., & Luong, M. 2009, *E&PSL*, **278**, 361
Barnes, J. W., Quarles, B., Lissauer, J. J., Chambers, J., & Hedman, M. M. 2016, *AsBio*, **16**, 487
Barnes, R. 2017, *CeMDA*, **129**, 509
Barnes, R., Jackson, B., Greenberg, R., & Raymond, S. N. 2009, *ApJL*, **700**, L30
Barnes, R., Luger, R., Deitrick, R., et al. 2020, *PASP*, **132**, 1008
Barnes, R., Mullins, K., Goldblatt, C., et al. 2013, *AsBio*, **13**, 225
Barnes, R., Raymond, S. N., Greenberg, R., Jackson, B., & Kaib, N. A. 2010, *ApJL*, **709**, L95
Batenburg, S. J., De Vleeschouwer, D., Sprovieri, M., et al. 2016, *ChiPa*, **12**, 1995
Batygin, K., & Laughlin, G. 2008, *ApJ*, **683**, 1207
Bills, B. G. 2005, *JGRE*, **110**, E11007
Blanco-Cuaresma, S., & Bolmont, E. 2017, Studying Tidal Effects In Planetary Systems With Posidonius. A N-Body Simulator Written In Rust, Zenodo, doi:10.5281/zenodo.1095095
Bolmont, E., Demory, B. O., Blanco-Cuaresma, S., et al. 2020, *A&A*, **635**, A117
Bolmont, E., Libert, A.-S., Leconte, J., & Selsis, F. 2016, *A&A*, **591**, A106
Bolmont, E., Raymond, S. N., Leconte, J., Hersant, F., & Correia, A. C. M. 2015, *A&A*, **583**, A116
Bolmont, E., Raymond, S. N., von Paris, P., et al. 2014, *ApJ*, **793**, 3
Boulila, S., Galbrun, B., Laskar, J., & Pálke, H. 2012, *E&PSL*, **317**, 273
Brasser, R., Morbidelli, A., Gomes, R., Tsiganis, K., & Levison, H. F. 2009, *A&A*, **507**, 1053
Bullock, M. A., & Grinspoon, D. H. 1996, *JGR*, **101**, 7521
Chambers, J. 2014, *Sci*, **344**, 479
Chambers, J. E. 1999, *MNRAS*, **304**, 793
Correia, A. C. M., Boué, G., & Laskar, J. 2012, *ApJL*, **744**, L23
Cumming, A., Butler, R. P., Marcy, G. W., et al. 2008, *PASP*, **120**, 531
Davies, J. H., & Davies, D. R. 2010, *SolE*, **1**, 5
De Vleeschouwer, D., Da Silva, A.-C., Sinnesael, M., et al. 2017, *NatCo*, **8**, 2268
Desch, S. J., Kalyaan, A., & O'D. Alexander, C. M. 2018, *ApJS*, **238**, 11
Dobrovolskis, A. R., & Ingersoll, A. P. 1980, *Icar*, **41**, 1
Dong, C., Huang, Z., Lingam, M., et al. 2017, *ApJL*, **847**, L4
Donohoe, A., Marshall, J., Ferreira, D., & Mcgee, D. 2013, *Jcli*, **26**, 3597
Dressing, C. D., Spiegel, D. S., Scharf, C. A., Menou, K., & Raymond, S. N. 2010, *ApJ*, **721**, 1295
Driscoll, P. E., & Barnes, R. 2015, *AsBio*, **15**, 739
Dumoulin, C., Tobie, G., Verhoeven, O., Rosenblatt, P., & Rambaux, N. 2017, *JGRE*, **122**, 1338
Duncan, M. J., & Quinn, T. 1993, *ARA&A*, **31**, 265
Egbert, G. D., & Ray, R. D. 2000, *Natur*, **405**, 775
Egbert, G. D., & Ray, R. D. 2003, *GeoRL*, **30**, 1907
Eggleton, P. P., Kiseleva, L. G., & Hut, P. 1998, *ApJ*, **499**, 853

- Ehlers, J., & Gibbard, P. 2007, *QuInt*, 164–165, 6
- Ehrenreich, D., Vidal-Madjar, A., Widemann, T., et al. 2012, *A&A*, 537, L2
- Folkner, W. M., Williams, J. G., Boggs, D. H., Park, R. S., & Kuchynka, P. 2014, IPNPR, 42–196, 1
- Ford, E. B. 2014, *PNAS*, 111, 12616
- Fukuhara, T., Futaguchi, M., Hashimoto, G. L., et al. 2017, *NatGe*, 10, 85
- Gilmore, J. B., & Ross, A. 2008, *PhRvD*, 78, 124021
- Goldblatt, C. 2015, *AsBio*, 15, 362
- Goldreich, P., & Soter, S. 1966, *Icar*, 5, 375
- Gomes, R., Levison, H. F., Tsiganis, K., & Morbidelli, A. 2005, *Natur*, 435, 466
- Gómez-Leal, I., Kaltenegger, L., Lucarini, V., & Lunkeit, F. 2018, *ApJ*, 869, 129
- Gough, D. O. 1981, *SoPh*, 74, 21
- Green, J. A. M., Way, M. J., & Barnes, R. 2019, *ApJL*, 876, L22
- Gronoff, G., Arras, P., Baraka, S. M., et al. 2020, *JGRA*, 125, e27639
- Hahn, J. M., & Malhotra, R. 1999, *AJ*, 117, 3041
- Hahn, J. M., & Malhotra, R. 2005, *AJ*, 130, 2392
- Hamano, K., Abe, Y., & Genda, H. 2013, *Natur*, 497, 607
- Hay, H. C. F. C., & Matsuyama, I. 2017, *Icar*, 281, 342
- Hay, J. D., Imbrie, J., & Shackleton, N. J. 1976, *Sci*, 194, 1121
- Heller, R., Leconte, J., & Barnes, R. 2011, *A&A*, 528, A27
- Hill, M. L., Kane, S. R., Seperuelo Duarte, E., et al. 2018, *ApJ*, 860, 67
- Horner, J., & Jones, B. W. 2008, *IJASB*, 7, 251
- Horner, J., & Jones, B. W. 2009, *IJASB*, 8, 75
- Horner, J., & Jones, B. W. 2012, *IJASB*, 11, 147
- Horner, J., Mousis, O., Petit, J. M., & Jones, B. W. 2009, *P&SS*, 57, 1338
- Horner, J., Vervoort, P., Kane, S. R., et al. 2020, *AJ*, 159, 10
- Howe, A. R., Adams, F. C., & Meyer, M. R. 2020, *ApJ*, 894, 130
- Hut, P. 1981, *A&A*, 99, 126
- Ingersoll, A. P., & Dobrovolskis, A. R. 1978, *Natur*, 275, 37
- Jackson, B., Barnes, R., & Greenberg, R. 2008a, *MNRAS*, 391, 237
- Jackson, B., Greenberg, R., & Barnes, R. 2008b, *ApJ*, 681, 1631
- Jagoda, M., Rutkowska, M., Kraszewska, K., & Suchocki, C. 2018, *StGG*, 62, 586
- Johnson, J. A., Aller, K. M., Howard, A. W., & Crepp, J. R. 2010, *PASP*, 122, 905
- Kane, S. R., Arney, G., Crisp, D., et al. 2019, *JGRE*, 124, 2015
- Kane, S. R., Barclay, T., & Gelino, D. M. 2013, *ApJL*, 770, L20
- Kane, S. R., Ciardi, D. R., Gelino, D. M., & von Braun, K. 2012, *MNRAS*, 425, 757
- Kane, S. R., & Gelino, D. M. 2012, *AsBio*, 12, 940
- Kane, S. R., Hill, M. L., Kasting, J. F., et al. 2016, *ApJ*, 830, 1
- Kane, S. R., Kopparapu, R. K., & Domagal-Goldman, S. D. 2014, *ApJL*, 794, L5
- Kane, S. R., & Torres, S. M. 2017, *AJ*, 154, 204
- Kasting, J. F. 1988, *Icar*, 74, 472
- Kasting, J. F., Chen, H., & Kopparapu, R. K. 2015, *ApJL*, 813, L3
- Kasting, J. F., Pollack, J. B., & Ackerman, T. P. 1984, *Icar*, 57, 335
- Kasting, J. F., Whitmire, D. P., & Reynolds, R. T. 1993, *Icar*, 101, 108
- Kent, D. V., Olsen, P. E., Rasmussen, C., et al. 2018, *PNAS*, 115, 6153
- Konopliv, A. S., & Yoder, C. F. 1996, *GeoRL*, 23, 1857
- Kopparapu, R. K., Ramirez, R., Kasting, J. F., et al. 2013, *ApJ*, 765, 131
- Kopparapu, R. K., Ramirez, R. M., SchottelKotte, J., et al. 2014, *ApJL*, 787, L29
- Kuhnt, W., Luderer, F., Nederbragt, S., Thurow, J., & Wagner, T. 2005, *IJEAS*, 94, 147
- Kulikov, Y. N., Lammer, H., Lichtenegger, H. I. M., et al. 2006, *P&SS*, 54, 1425
- Kulikov, Y. N., Lammer, H., Lichtenegger, H. I. M., et al. 2007, *SSRv*, 129, 207
- Lammer, H., Kasting, J. F., Chassefière, E., et al. 2008, *SSRv*, 139, 399
- Laskar, J. 1988, *A&A*, 198, 341
- Laskar, J., Boué, G., & Correia, A. C. M. 2012, *A&A*, 538, A105
- Laskar, J., Fienga, A., Gastineau, M., & Manche, H. 2011, *A&A*, 532, A89
- Laskar, J., Robutel, P., Joutel, F., et al. 2004, *A&A*, 428, 261
- Laurin, J., Meyers, S. R., Galeotti, S., & Lanci, L. 2016, *E&PSL*, 442, 143
- Leconte, J., Chabrier, G., Baraffe, I., & Levrard, B. 2010, *A&A*, 516, A64
- Leconte, J., Forget, F., Charnay, B., Wordsworth, R., & Pottier, A. 2013, *Natur*, 504, 268
- Levison, H. F., & Agnor, C. 2003, *AJ*, 125, 2692
- Levison, H. F., Morbidelli, A., Van Laerhoven, C., Gomes, R., & Tsiganis, K. 2008, *Icar*, 196, 258
- Lichtenegger, H. I. M., Kislyakova, K. G., Odert, P., et al. 2016, *JGRA*, 121, 4718
- Lincowski, A. P., Lustig-Yaeger, J., & Meadows, V. S. 2019, *AJ*, 158, 26
- Lisiecki, L. E. 2014, *PalOc*, 29, 71
- Luger, R., & Barnes, R. 2015, *AsBio*, 15, 119
- Lustig-Yaeger, J., Meadows, V. S., & Lincowski, A. P. 2019, *ApJL*, 887, L11
- Lykawka, P. S., Horner, J., Jones, B. W., & Mukai, T. 2009, *MNRAS*, 398, 1715
- Lykawka, P. S., Horner, J., Jones, B. W., & Mukai, T. 2010, *MNRAS*, 404, 1272
- Mai, C., Desch, S. J., Kuiper, R., Marleau, G.-D., & Dullemond, C. 2020, *ApJ*, 899, 54
- Malhotra, R. 1993, *Natur*, 365, 819
- Malhotra, R. 1995, *AJ*, 110, 420
- Malhotra, R. 2019, *GSL*, 6, 12
- Martinez, M., & Dera, G. 2015, *PNAS*, 112, 12604
- Mignard, F. 1979, *M&P*, 20, 301
- Minton, D. A., & Malhotra, R. 2009, *Natur*, 457, 1109
- Morbidelli, A., Brasser, R., Gomes, R., Levison, H. F., & Tsiganis, K. 2010, *AJ*, 140, 1391
- Morbidelli, A., Levison, H. F., Tsiganis, K., & Gomes, R. 2005, *Natur*, 435, 462
- Navarro, T., Schubert, G., & Lebonnois, S. 2018, *NatGe*, 11, 487
- Neron de Surgy, O., & Laskar, J. 1997, *A&A*, 318, 975
- Nesvorný, D. 2018, *ARA&A*, 56, 137
- Nesvorný, D., Vokrouhlický, D., Bottke, W. F., & Levison, H. F. 2018, *NatAs*, 2, 878
- Nielsen, L. D., Gandolfi, D., Armstrong, D. J., et al. 2020, *MNRAS*, 492, 5399
- Noyelles, B., Frouard, J., Makarov, V. V., & Efroimsky, M. 2014, *Icar*, 241, 26
- O'Brien, D. P., Walsh, K. J., Morbidelli, A., Raymond, S. N., & Mandell, A. M. 2014, *Icar*, 239, 74
- Ostberg, C., & Kane, S. R. 2019, *AJ*, 158, 195
- Palubski, I., Shields, A., & Deitrick, R. 2020, *ApJ*, 890, 30
- Pirani, S., Johansen, A., Bitsch, B., Mustill, A. J., & Turrini, D. 2019, *A&A*, 623, A169
- Pognan, Q., Garraffo, C., Cohen, O., & Drake, J. J. 2018, *ApJ*, 856, 53
- Popp, M., Schmidt, H., & Marotzke, J. 2016, *NatCo*, 7, 10627
- Pozuelos, F. J., Suárez, J. C., de Elía, G. C., et al. 2020, arXiv:2006.09403
- Ramirez, R. M. 2018, *Geosc*, 8, 280
- Ramirez, R. M. 2020, *MNRAS*, 494, 259
- Ramirez, R. M., & Kaltenegger, L. 2014, *ApJL*, 797, L25
- Raymond, S. N., & Izidoro, A. 2017, *Icar*, 297, 134
- Raymond, S. N., Kokubo, E., Morbidelli, A., Morishima, R., & Walsh, K. J. 2014, in *Protostars and Planets VI*, ed. H. Beuther et al. (Tucson, AZ: Univ. Arizona Press), 595
- Raymond, S. N., & Morbidelli, A. 2020, arXiv:2002.05756
- Raymond, S. N., Quinn, T., & Lunine, J. I. 2006, *Icar*, 183, 265
- Renaud, J. P., & Henning, W. G. 2018, *ApJ*, 857, 98
- Ribas, I., Guinan, E. F., Güdel, M., & Audard, M. 2005, *ApJ*, 622, 680
- Roig, F., Nesvorný, D., & DeSouza, S. R. 2016, *ApJL*, 820, L30
- Schaefer, L., & Fegley, B. J. 2011, *ApJ*, 729, 6
- Schiller, M., Bizzarro, M., & Fernandes, V. A. 2018, *Natur*, 555, 507
- Taylor, F., & Grinspoon, D. 2009, *JGRE*, 114, E00B40
- Taylor, F. W., Svedhem, H., & Head, J. W. 2018, *SSRv*, 214, 35
- Titov, D. V., Bullock, M. A., Crisp, D., et al. 2007, *GMS*, 176, 121
- Tsiganis, K., Gomes, R., Morbidelli, A., & Levison, H. F. 2005, *Natur*, 435, 459
- Turcotte, D. L., & Schubert, G. 2002, *Geodynamics* (Cambridge: Cambridge Univ. Press)
- Walsh, K. J., Morbidelli, A., Raymond, S. N., O'Brien, D. P., & Mandell, A. M. 2011, *Natur*, 475, 206
- Walsh, K. J., Morbidelli, A., Raymond, S. N., O'Brien, D. P., & Mandell, A. M. 2012, *M&PS*, 47, 1941
- Way, M. J., & Del Genio, A. D. 2020, *JGRE*, 125, e06276
- Way, M. J., Del Genio, A. D., Kiang, N. Y., et al. 2016, *GeoRL*, 43, 8376
- Way, M. J., & Georgakarakos, N. 2017, *ApJL*, 835, L1
- Williams, D. M., & Pollard, D. 2002, *IJASB*, 1, 61
- Winn, J. N., & Fabrycky, D. C. 2015, *ARA&A*, 53, 409
- Wittenmyer, R. A., Wang, S., Horner, J., et al. 2020, *MNRAS*, 492, 377
- Wolf, E. T., & Toon, O. B. 2014, *GeoRL*, 41, 167
- Wordsworth, R. D., & Pierrehumbert, R. T. 2013, *ApJ*, 778, 154
- Zahnle, K. J., & Kasting, J. F. 1986, *Icar*, 68, 462
- Zeebe, R. E. 2015, *ApJ*, 798, 8